Effect of the Y955C Mutation on Mitochondrial DNA Polymerase Nucleotide Incorporation Efficiency and Fidelity

ARTICLE *in* BIOCHEMISTRY · JUNE 2011

Impact Factor: 3.02 · DOI: 10.1021/bi200280r · Source: PubMed

2 AUTHORS, INCLUDING:

Patricia Estep
Adimab, LLC
6 PUBLICATIONS **38** CITATIONS

SEE PROFILE

Published in final edited form as:
Biochemistry. 2011 July 26; 50(29): 6376–6386. doi:10.1021/bi200280r.

Effect of the Y955C Mutation on Mitochondrial DNA Polymerase Nucleotide Incorporation Efficiency and Fidelity

Patricia A. Estep and **Kenneth A. Johnson***
University of Texas at Austin, Department of Chemistry & Biochemistry, Institute of Cellular and Molecular Biology, 2500 Speedway, Austin, TX 78712

Abstract

The human mitochondrial DNA polymerase (pol γ) is responsible for the replication of the mitochondrial genome. Mutation Y955C in the active site of pol γ results in early onset progressive external ophthalmoplegia, premature ovarian failure, and Parkinson's disease. In single turnover kinetic studies, we show that the Y955C mutation resulted in a decrease in the maximum rate of polymerization and an increase in the K_m for correct incorporation. The mutation decreased the specificity constant for correct incorporation of dGTP, TTP, and ATP to values of 1.5, 0.35, and 0.044 $\mu M^{-1}s^{-1}$, respectively, representing reductions of 30-, 110- and 1300-fold relative to wild-type enzyme. The fidelity of incorporation was reduced 6- to 130-fold; largely due the significant decrease in the specificity constant for correct dATP:T incorporation. For example, k_{cat}/K_m for forming a TTP:T mismatch was decreased tenfold from 0.0002 to 0.00002 $\mu M^{-1}s^{-1}$ by the Y955C mutant, but the 1300-fold slower incorporation of the correct dATP:T relative to wild-type led to a 130-fold lower fidelity. While correct incorporation of 8-oxo-dGTP was largely unchanged, incorporation of 8-oxo-dG with dA in the template strand was reduced 500-fold. These results support a role of Y955 in stabilizing A:T base pairs at the active site of pol γ and suggest that the severe clinical symptoms of patients with this mutation may be due, in part, to the reduced efficiency of dATP incorporation opposite T, and that the autosomal dominant phenotype may arise from the resulting higher mutation frequency.

Understanding the molecular basis for disease has become an increasingly important part of biochemical studies as genetic testing becomes more common. Identification of the proteins or genes responsible for a particular disease could allow for better treatments and/or earlier intervention. Deletions or mutations in human mitochondrial DNA polymerase (pol γ) have been correlated with various mitochondrial disorders, including mtDNA depletion syndrome, Alpers Syndrome, and progressive external opthamalplegia (PEO) (1). Symptoms of Alpers Syndrome include liver disease and refractory seizures, while patients with PEO present with progressive weakness of the external ocular muscles and skeletal myopathy (2, 3).

Mitochondrial DNA (mtDNA) replication is performed by a replisome comprised of a nuclearly-encoded catalytic subunit, two subunits of the processivity factor (p55), the single-stranded DNA binding protein, and a DNA helicase (4). The crystal structure of the holoenzyme, a heterotrimer comprised of the catalytic subunit of the polymerase and a dimer of p55, was recently solved (5). Like other Family A polymerases, the mtDNA polymerase structure resembles a right hand comprised of thumb, fingers, and palm domains. Recent studies on two other A family polymerases, HIV reverse transcriptase and T7 DNA polymerase, have guided our work on pol γ, providing insight into the mechanism

CORRESPONDING AUTHOR: Kenneth A. Johnson, Department of Chemistry & Biochemistry, Institute for Cellular and Molecular Biology, The University of Texas, Austin, Texas 78712, kajohnson@mail.utexas.edu, Phone: 512-471-0434, Fax: 512-471-0435.

of catalysis as well as the potential mechanisms of discrimination against incorrect nucleotides and the role of nucleotide-induced conformational changes in selectivity (6, 7). The pathway of nucleotide incorporation can be simplified to that shown in Scheme 1, where ED_n represents a complex of enzyme with DNA that is n bases long, and N represent a nucleoside triphosphate.

In this simplified scheme, the ground-state binding is represented by the term $1/K_1$ (K_d), while the rate of chemistry is described by k_{pol}. Normally pyrophosphate release and translocation to allow the binding of the next nucleotide are much faster than incorporation (8–10). Accordingly, the rate of incorporation measured in a single turnover experiment defines the kinetics governing sequential nucleotide incorporation events during processive synthesis. Accordingly, the values of k_{pol}/K_d measured in single turnover kinetic studies define k_{cat}/K_m for processive synthesis. Moreover, the apparent K_d measured in these studies should be more generally described as a K_m value, which approaches a true K_d when the chemistry step is slow (6, 7). Throughout the text, we will refer to the results from our single turnover kinetic studies in terms of k_{cat} and K_m values to eliminate the misconception that the results define K_d.

The crystal structure of the ternary complex of pol γ has yet to be solved, and so comparisons between pol γ and T7 DNA polymerase have been helpful in identifying the potential roles of particular residues. As summarized in Fig. 1, catalytic residues are conserved in comparing T7 DNA polymerase and pol γ thereby allowing homology modeling based upon the T7 DNA polymerase ternary E-DNA-nucleotide complex (11, 12) to suggest possible interactions at the active site. Within the active site of pol γ, homology suggests that residue R943 contacts the γ phosphate, while Y951 and H932 each contact the β-phosphate, leaving K947 to make contact with the α-phosphate, as confirmed by recent mutagenesis studies (13). Tyrosine 955 is not involved directly in contacts with the phosphate backbone; rather, it appears that it participates in a hydrogen-bonding network involving a glutamate residue in the palm of the enzyme (E895 in pol γ, not shown). This hydrogen-bond network may be essential not only for maintaining the architecture of the polymerase active site but also for the recognition of the correct incoming nucleotide. Mutation of Y530 to a phenylalanine in T7 DNAP resulted in a loss of discrimination through a lower affinity for the incoming nucleotide rather than a decrease in the rate of polymerization (14).

Autosomal dominant forms of PEO usually involve mutations in pol γ that are in the active site of the polymerase. Patients with the Y955C mutation present with early onset autosomal dominant PEO in their thirties (15). These patients often later present with Parkinson's disease and in women, premature ovarian failure (15–17). MtDNA in skeletal muscle cells of these patients shows some deletions, though a large proportion of the mtDNA is intact, indicating some level of complete replication by the polymerase (17). In yeast, a mutant of Mip1 homologous to the human polymerase gamma mutant Y955C leads to increased petite frequency, suggesting mitochondria malfunction (18). In addition, qualitative studies have shown that both the mutation and deletion frequency are increased with this mutant (3, 19).

Oxidatively damaged guanosine, in the form of 8-oxo-deoxyguanosine, accumulates in the mitochondria and contributes to the formation of mutations (20). The 8-oxo-dG can base pair with either a cytosine in the *anti*-conformation or with an adenosine in the *syn*-conformation, leading to frequent mutations (21). Pol γ uses a novel mechanism to reduce the rate of incorporation of 8-oxo-dGTP by slowing the rate of pyrophosphate release allowing the chemical reaction to come to equilibrium at the enzyme active site (21). Therefore, it is important to establish which residues are responsible for this slow pyrophosphate release, as they affect discrimination against 8-oxo-dGTP. Therefore we have

examined the kinetics of incorporation by the Y955C mutant as part of this study. Moreover, if the Y955C mutant incorporated 8-oxo-dGTP at a higher rate, that could account for the observed physiological effects of this mutation.

Understanding the molecular basis for diseases linked to mtDNA replication requires accurate kinetic analysis to quantify the effects of the mutation. Although many mutations in pol γ have been characterized previously (12, 22, 23), we show in this study that the published results are unreliable. Our new results provide a basis to correlate the biochemistry of mtDNA replication with physiology.

Materials and Methods

Cloning and Plasmid Construction for the Large Subunit of Polymerase γ (p140)

The creation of the Y955C mutant on an exonuclease deficient background (D198A/E200A) on the pUC19 plasmid (New England Biolabs) was performed using two-step PCR using primers flanking SacII and NotI restriction sites. The mutagenic primers used were the following: 5′ CAA TTA CGG TCG TAT TTG CGC GCA GGT CAG CCG 3′, complementary strand: 5′ GCT GAC CTG CGC CGC AAA TAC GAC CGT AAT TGA AAA T 3′. The SacII and NotI restriction sites were used to insert the PCR-generated fragment into the gene. A NotI/BglII digest was then used to remove the gene from pUC19.1 for ligation into the pBacPak9 vector (Clontech). Creation of baculovirus containing the gene for Y955C pol γ was as previously described (13).

Purification of Small Subunit (p55) and Polymerase γ Y955C mutants

The small subunit (p55) was expressed using the pET43.1a vector with a histidine-tag in *E. coli* Rosetta 2 (DE3) and then purified as previously described (13). For purification of the large subunit of the polymerase with the Y955C mutation, the cells were lysed by re-suspension in a buffer containing 0.32 M Sucrose, 10 mM HEPES (pH 7.5), 3 mM $CaCl_2$, 2 mM MgAc•$4H_20$, 0.1 mM EDTA. Protease Inhibitor Cocktail IV (EDTA-free, AG Scientific) was added to the lysis buffer. The lysate was clarified by centrifugation at 1,500 × g for 15 minutes. DNA was removed by increasing the salt to a final [KCl] of 0.5 M. The lysate was again centrifuged in a Beckman Coulter Ultracentrifuge at 31,000 × g in a Ti45 rotor. Next, the lysate was subjected to a Ni-NTA column (QIAgen) via the batch method. The protein was bound to the resin pre-equilibrated with 20 mM HEPES (pH 7.5), 5 mM imidazole, 200 mM KCl, and 5% glycerol by stirring on ice. The beads were collected via centrifugation at 1500 × g for 10 minutes, and then washed with 20 mM HEPES (pH 7.5), 200 mM KCl, 20 mM imidazole, 5% glycerol. The beads were then poured into a column and the protein was eluted with 20 mM HEPES (pH 7.5), 100 mM KCl, 200 mM imidazole, 5% glycerol. The fractions containing the polymerase were pooled and diluted before loading onto an SP Sepharose column (Amersham Biosciences) with a flow rate of 1ml/min in buffer A containing 20 mM HEPES (pH 7.5), 30 mM KCl, 1 mM DTT, 1 mM EDTA, 5% glycerol. Buffer B contained 20 mM HEPES (pH 7.5), 700 mM KCl, 1mM DTT, 1 mM EDTA, 5% glycerol. The protein was eluted with a step-gradient from 0–100% B. The fractions containing polymerase gamma were pooled, concentrated via a centrifugal concentrator with a 50 kDa cutoff (GE Healthcare), and dialyzed against the final storage buffer containing 50 mM Tris-HCl (pH 8.4), 100 mM NaCl, 1 mM DTT, 50% glycerol. Concentrations of active enzyme were obtained by active site titration of the burst amplitude versus DNA concentration.

Preparation of DNA

Oligonucleotides were purchased from IDT DNA Technologies and purified using 15% acrylamide/7M Urea denaturing PAGE gels. A 25-mer primer and a 45-mer template

(Template 1 shown in Table I) were adopted from previous studies for misincorporation assays (13). Templates 2 and 3 were used for incorporation assays involving 8-oxo-dGTP. The 25-mer was 5′ ^{32}-P labeled with T4 polynucleotide kinase as recommended by the manufacturer (New England Biolabs). Excess γ-^{32}-P –ATP was removed by a Bio-Spin 6 gel filtration column (BioRad), and the amount of labeled DNA was quantified by TLC. The labeled 25-mer and unlabeled 45-mer were mixed in a 1:1 molar ratio and annealed by heating to 95 degrees for 5 minutes, followed by slow cooling to room temperature.

Single Turnover Experiments

All experiments were performed at 37° C in a solution containing 50 mM Tris-HCl (pH 7.5), 100 mM NaCl, and 12.5 mM $MgCl_2$.. To eliminate complications of multiple turnovers, reactions were performed under single turnover conditions, with enzyme in excess and limiting DNA substrate. For fast reactions, assays were performed with a KinTek RQF-3 Rapid Quench Flow apparatus. For both correct incorporation and misincorporation assays, the holoenzyme (200 nM to 300 nM large subunit and 0.8 to 1.2 μM small subunit) were pre-incubated with 25/45-mer DNA (140 nM-200 nM) in reaction buffer without magnesium chloride and loaded into one syringe. The other syringe contained the nucleotide (0.5 μM to 500 μM for correct incorporation, and 25 μM to 5 mM for incorrect incorporation) in reaction buffer with magnesium chloride. After rapid mixing, the reaction was quenched with 0.5 M EDTA. Misincorporation assays requiring longer time points were performed by manual mixing. Reactions involving 8-oxo-dGTP were performed with either rapid quenching or hand quenching with concentrations varying from 1 μM to 1 mM 8-oxo-dGTP.

The products were resolved on 15% acrylamide/7M denaturing PAGE gels. The gels were dried and exposed to a PhosphorImager screen. The screen was then scanned by a Typhoon Scanner (GE Healthcare Life Sciences) to reveal product bands. The amount of product (26-mer) was quantified versus the amount of starting material to determine fraction of product.

Global Fitting

All data were fit globally based upon numerical integration of rate equations using the KinTek Explorer program (KinTek Corporation) (24, 25). Nonlinear regression was used to find optimal parameters in fitting each set of data to a single model. While fitting data, previously estimated rates of DNA binding and release were used in constructing a comprehensive model including all known steps. For example, Scheme 1 was expanded to:

$$E+D_n \underset{k_{off}}{\overset{k_{on}}{\rightleftarrows}} ED_n$$

$$ED_n+N \underset{k_{-1}}{\overset{k_1}{\rightleftarrows}} ED_nN \overset{k_2}{\rightleftarrows} ED_{n+1}+PP_i$$

The DNA binding and dissociation rates for both substrate and product DNA (D_n, D_{n+1}) were set to be k_{on} = 20 $\mu M^{-1}s^{-1}$ and k_{off} = 0.02 s^{-1} to satisfy the steady state DNA release rate and the $K_{d,DNA}$ of 10 nM (26). The rate of nucleotide binding is thought to be limited by diffusion, so k_1 was set to 100 $\mu M^{-1}s^{-1}$. By allowing the dissociation rate to vary (k_{-1}), the equilibrium constant was calculated, $K_1 = k_1/k_{-1}$. Thus, to fit a full concentration series, only k_{-1} and k_2 were adjust to fit the family of curves and thereby define the apparent K_d (K_m) and k_{pol} (k_{cat}), respectively. To account for slight variations in the data, enzyme or DNA concentration were adjusted slightly (±10%) to derive best fits. Standard error estimates were obtained by nonlinear regression and were checked using confidence contour analysis. The upper and lower limits were derived based on a chi^2 threshold of 20%, as

previously described (25). In all cases, the error estimates derived by nonlinear regression were similar to the estimates based upon the confidence contour analysis, verifying that the parameters were well constrained.

In presenting the results in each of the figures, data at long times were omitted from the graph in order to illustrate more clearly the data at shorter times. Although not displayed, data at longer times were included in the data fitting. In particular, the longer time points help to define the amplitude of the reactions at the lower concentrations as part of the global fitting.

A note on nomenclature

We reserve the term, “rate constant” to only refer to an “intrinsic rate constant” for an individual step in a reaction pathway (i.e., that represented by a lower case k over an arrow). Moreover, we see little utility in the distinction between a rate derived by an initial velocity (slope as the change in product with time) and a rate measured by fitting to an exponential function and do not adhere to the standard that the latter should be referred to as a “rate constant.” Although clearly having distinct meanings and units, both are methods to measure the rate of a reaction. Moreover, it is often misleading to presume that an Eigenvalue derived by fitting data to an exponential function is an intrinsic rate constant. In the process of fitting data, we derive rates of reaction in units of s^{-1}, and because these measurements do not necessarily resolve individual rate constants, we refer to them as rate measurements.

Free energy of discrimination

Discrimination against each mismatch was calculated from:

$$D\frac{(k_{cat}/K_m)_{correct}}{(k_{cat}/K_m)_{mismatch}}$$

which is equal to the reciprocal of the frequency of misincorporation (fidelity). We computed the apparent change in free energy due to the Y955C mutation reflected in the changes in k_{cat} and K_m according to the following equations:

$$\Delta\Delta G_c = -RT\ln\left(\frac{k_{cat}^{Y955C}}{k_{cat}^{wt}}\right)$$

$$\Delta\Delta G_m = -RT\ln\left(\frac{K_m^{wt}}{K_m^{Y955C}}\right)$$

The net change in the specificity constant is the sum of the contributions from k_{cat} and K_m on the free energy scale.

Calculation of k_{cat} and K_m

After fitting data in Fig. 5C to Scheme 2, we computed k_{cat} and K_m from the following:

$$k_{cat}=\frac{k_2k_3}{k_2+k_{-2}+k_3}$$
$$K_m=\frac{k_2k_3+k_{-1}(k_{-2}+k_3)}{k_1(k_2+k_{-2}+k_3)}$$
$$k_{cat}/K_m=k_1\frac{k_2k_3}{k_2k_3+k_{-1}(k_{-2}+k_3)}$$

Results

Kinetics of single nucleotide incorporation measured by quench-flow experiments

Single-nucleotide incorporation experiments were performed to determine the parameters for correct nucleotide incorporation by the Y955C mutant. The experiments were performed under single-turnover conditions in that the concentration of enzyme exceeded the concentration of DNA. The nucleotide concentration dependence of the rate was analyzed to provide estimates of an apparent dissociation constant ($K_{d,app} = K_m$) and a maximum rate of nucleotide incorporation, ($k_{pol} = k_{cat}$) according to Scheme 1. Fig. 2 shows the time dependence of product formation at several nucleotide concentrations to define the kinetics of incorporation of dATP:T, dGTP:dC and TTP:dA. To avoid confusion, we use the notation dATP:T to represent the incorporation of dATP opposite a template T, for example. The data in the experiment were globally fit to the mechanism shown in Scheme 1 based upon numerical integration of the rate equations to obtain values for the apparent nucleotide dissociation constant and the maximum rate of incorporation (24).

Several underlying assumptions govern the fitting of the data to the model in Scheme 1. Ground state nucleotide binding is thought to occur as a rapid equilibrium, which was modeled with the initial collision of the nucleotide and enzyme occurring at a rate limited by diffusion (100 $\mu M^{-1}s^{-1}$) in order to define an apparent dissociation constant, $K_{d,app}$ (K_m). Second, the rate-limiting step is believed to be polymerization, while conformational changes preceding chemistry, pyrophosphate release and translocation are thought to be fast, based upon more detailed studies on homologous enzymes (6, 7). Accordingly, the ratio of $k_{pol}/K_{d,app}$ defines k_{cat}/K_m, the specificity constant governing sequential nucleotide incorporation events during processive synthesis.

The kinetic parameters for correct incorporation are summarized in Table 2 and compared to the values for wild-type enzyme (27). The Y955C mutation affected not only the rate of polymerization, dropping as much as a factor of 20, but k_{cat}/K_m was greatly affected. The effect on k_{cat}/K_m was most severe with dATP:T base pairs, mostly due to much weaker nucleotide binding. As summarized in Table 2, the Y955C mutation caused a 1300-fold reduction in kcat/Km for incorporation of dATP:T, while the effects on TTP:dA and dGTP:dC were only 110-and 30-fold, respectively.

Kinetics of misincorporation

The kinetics of misincorporation were measured to investigate the discrimination against mismatches by the Y955C mutant compared to the wild-type enzyme. In particular, we examined the incorporation of dCTP, TTP, and dGTP opposite a templating T. In many cases, multiple nucleotides were incorporated onto the primer strand such that products up to 32 nucleotides long were observed (see Fig. 3). When quantifying the product, all of the extended primers were included in the total concentration of product formed in order to define the rate of formation of the first mismatch. The concentration of product was plotted as a function of time (Fig. 4), and then fit globally to Scheme 1 to get the kinetic parameters listed in Table 3. The kinetic parameters for misincorporation for the wild-type enzyme were determined previously (28) and are listed for comparison. As shown in Table 3, there is a

significant decrease in fidelity, 6-, 26, 120- and 50-fold for dGTP:T, dCTP:T, TTP:T and dGTP:dA mismatches, respectively.

Incorporation of 8-oxo-dGTP

The kinetics of incorporation of 8-oxo-dGTP were measured under single turnover conditions opposite a dCMP or dAMP templating base. The formation of product over time is shown in Figs. 5A and 5B, and fit to Scheme 1 to get the results summarized in Table 4. These data show no significant change in k_{cat}/K_m for incorporation of 8-oxo-dGTP opposite a template dC, but a 500-fold reduction for incorporation opposite a template dA, compared to wild-type.

It was important to evaluate whether the kinetics of incorporation of 8-oxo-dGTP followed the more complex pattern seen with the wild-type enzyme. That is, with the wild-type enzyme the kinetics show a clear nucleotide concentration dependence of amplitude as shown in Fig. 5C, reproduced from (21). Incorporation of 8-oxo-dGTP by the wild-type enzyme follows Scheme 2, with a slow pyrophosphate release leading to accumulation of the product complex ($ED_{n+1}PP_i$) in equilibrium with bound substrate. This leads to a distinct kinetic signature where the amplitude of the pre-steady state burst is dependent upon nucleotide concentration.

In Fig. 5C, we reproduce the data from the Hanes & Johnson 2006 paper, but now fit the data globally to the model shown in Scheme 2. Confidence contour analysis (Fig. 6B) justifies the fitting of the data to four rate constants by showing that all four rate constants are well constrained.

Incorporation of 8-oxo-dGTP opposite a templating dC by the Y955C mutant (Fig. 5B) does not show the same pattern as seen for the wild-type enzyme. That is, the curves for the Y955C mutant share the same end-point derived by fitting the data globally, and the data can be accounted for sufficiently by the model shown in Scheme 1. Thus, unlike the wild-type enzyme (Fig. 5C), the concentration dependence of incorporation of 8-oxo-dGTP by the mutant gave no evidence to suggest that the reaction was followed by slow pyrophosphate release. The rate of misincorporation of a 8-oxo-dGTP:dA base pair by the Y955C mutant was 500-fold slower (Table 4, $k_{cat}/K_m = 0.0004\ \mu M^{-1}s^{-1}$) than by the wild-type ($k_{cat}/K_m = 0.2\ \mu M^{-1}s^{-1}$); and thus, the mutant showed increased discrimination against misincorporation of 8-oxo-dGTP. The incorporation of 8-oxo-dGTP:dA was comparable to the rate of misincorporation of dGTP:dA (Table 3, $k_{cat}/K_m = 0.0003\ \mu M^{-1}s^{-1}$). Overall, the data suggest that the physiological effects of the Y955C mutation are not due to increased rates of incorporation of 8-oxo-dGTP.

Global Fitting/Contour analysis

Each set of curves was globally fit using the KinTek Explorer (24, 25). The global fitting routine is based on numerical integration of rate equations, allowing the parameters to be derived by directly fitting to a complete model. In this type of fitting, both the rate and the amplitude of the reaction are taken into account, eliminating the simplifications of equations and errors that are common during traditional fitting. This has proved useful in fitting data where there is a clear nucleotide concentration dependence of the amplitude, or data where the nucleotide concentration is comparable to that of enzyme. It is necessary to ensure that the model is not overly complex, and that the data are able to support the definition of each step in the model. We address this by performing confidence contour analysis, whereby the constants are systematically varied and we estimate the extent to which each parameter in a model is constrained by the data.

In contour analysis (Fig. 6A), the red zone represents a range of values that provide a good fit to the data given in Fig. 5A. The margin shown by the yellow band between the red and green zones defines a boundary that represents a 20% increase in *chi*^{2}, which is used to estimate the upper and lower confidence intervals on each of the parameters (25). In the case of 8-oxo-dGTP incorporation by the Y955C mutant (Fig. 5A), we can see that the parameters are well constrained by the data to support the mechanism shown in Scheme 1. The upper and lower confidence limits have been compared to the standard error estimates derived by nonlinear regression. Because the two methods of estimating errors agreed for the data reported here, we omitted the upper and lower limits from the Tables for clarity. Note also that the ratio of k_{cat}/K_m is known with greater certainty than either parameter, k_{cat} or K_m, as revealed by the linear relationship between k_2 and k_{-1} on the confidence contour. This is equivalent to stating that the slope of a rate versus concentration curve is known with greater certainty than the k_{cat}/K_m value computed from the ratio of the k_{cat} and K_m values.

In Fig. 6B, we show the confidence contours derived from global fitting of the data in Fig. 5C. This analysis demonstrates that all four rate constants were well constrained in fitting the data to Scheme 2 based upon simultaneously fitting the rate and amplitude dependence of the observed reaction. As summarized in the legend to Fig. 5, the rate constants derived by global fitting are comparable to those obtained by conventional analysis, but the error limits are better defined by the global fitting and the concentration dependence of the rate and amplitude are fit simultaneously, rather than separately.

Discussion

In all Family A polymerases, there is a tyrosine residue at the end of the helix containing several catalytic residues. Studies involving the T7 DNA polymerase have suggested that this residue plays a role in stabilizing the incoming nucleotide, with the phenyl ring of the tyrosine stacking with the nucleotide, and the hydroxyl group forming hydrogen bonds that help to stabilize the architecture of the active site (11). Mutation of the homologous residue (Y530) to phenylalanine in T7 DNA polymerase resulted in an increase in the dissociation constant for incoming nucleotides with only a modest effect on the rate of polymerization (14) and a corresponding decrease in fidelity. As shown here, the mutation of tyrosine to a cysteine has a much more drastic effect. In particular, we observe a 30- to 1300-fold reduction in k_{cat}/K_m governing correct base pair incorporation due to the Y955C mutation. In addition, there was a 6 to 120-fold reduction in fidelity. In contrast, there was little change in the kinetics of incorporation of 8-oxo-dGTP opposite a template dC, but a 500-fold improvement in discrimination against a 8-oxo-dGTP:dA mismatch.

Previous studies of the Y955C mutation based upon steady-state methods in the Copeland laboratory have provided inconsistent results (12, 29). For example, steady state measurements gave values of $k_{cat} = 0.05\ s^{-1}$, $K_m = 40$ nM, and $k_{cat}/K_m = 1.2\ \mu M^{-1}s^{-1}$ for incorporation of dGTP:dC by wild-type enzyme (30). In contrast, our methods provided values of $k_{cat} = 37\ s^{-1}$, $K_m = 0.8\ \mu M$, and $k_{cat}/K_m = 46\ \mu M^{-1}s^{-1}$ (Table 2). Thus, the specificity constant derived by steady state methods was 38-fold lower than what we observed in single turnover experiments. Comparing values for wild-type enzyme and the Y955C mutant reveals that the k_{cat}/K_m values derived by steady state methods in the Copeland laboratory were lower by factors ranging from 27- to 62,000-fold (30) compared to the results presented here. Most noteworthy, Copeland and his coworkers underestimated the rate of incorporation of 8-oxo-dGTP:dA by wild-type enzyme by a factor of 8,000-fold and thus they failed to properly assess the importance of mismatch formation with this oxidatively damaged nucleotide. In addition, they underestimated the specificity constant for incorporation of dGTP:dC by the Y955C mutation by 62,000-fold and accordingly overstated the magnitude of the defect. Similar discrepancies exist in the specificity

constants for incorporation of nucleoside analogs used to treat HIV infections in comparing the results from pre-steady state (31) and steady state kinetics (32). In comparing the published results from two papers from the Copeland lab (12, 29), k_{cat} values for wild-type enzyme were reported to be either 0.36 min^{-1} or 1.3 s^{-1}. This 220-fold variation in k_{cat} values reported for the wild-type enzyme engenders little confidence in the quality of data.

For DNA polymerases, steady state k_{cat} and K_m values are reduced by a factor approaching the processivity of the enzyme, which for pol γ is approximately 2,000 (26). Although, in theory, steady state measurements on a DNA polymerases should still provide a valid specificity constant (33) and may be adequate for enzymes with low processivity (34), in practice, experiments on pol γ would need to be designed to accurately measure a steady state K_m value of ~0.5 nM to accurately assess correct incorporation kinetics. As a counterargument, one might propose that the single turnover kinetics overestimate the rates because the first turnover might be faster than subsequent turnovers. However, experiments to measure the kinetics of sequential nucleotide incorporation on several DNA polymerases have shown that the rate of incorporation of each nucleotide is comparable to that measured in single turnover experiments (9, 27, 35). Moreover, there is no evidence for a kinetically significant step between sequential nucleotide incorporation events, implying that pyrophosphate release and translocation are normally much faster than incorporation. Direct measurements on pol γ demonstrated that pyrophosphate release was kinetically correlated with incorporation, implying fast pyrophosphate release after chemistry (36, 37). Thus, the rate constants derived from single turnover kinetic studies accurately define the parameters governing sequential nucleotide incorporation events during processive synthesis and avoid the complications introduced in steady state measurements of a processive DNA polymerase. Moreover, pre-steady state experiments provide important quality control for the concentration of active enzyme in a preparation from the measured amplitude of the reaction. In surveying the literature on pol γ, it is our opinion that the results of steady state kinetics, in general, and those from the Copeland lab in particular, are unreliable and conclusions based upon their quantitative results must be reevaluated.

Family A polymerases typically have a two-step binding mechanism, where a conformational change is a critical component of nucleotide recognition (6, 7, 38). Studies on T7 DNA polymerase and HIV RT have shown that this conformational change is fast and establishes the specificity constant for correct incorporation. However, when the chemistry step is slow, the conformational change comes to equilibrium before incorporation (6, 7). Without any method to measure the conformational change in pol γ, it is difficult to interpret whether the apparent K_d represents a true dissociation constant or simply reflects the ratio of k_{cat} and the net substrate binding rate. The issue is whether the binding steps come to equilibrium before the chemistry step. In either case, the apparent K_d provides an accurate estimate of the K_m governing single nucleotide incorporation during processive synthesis and k_{pol}/K_d defines the specificity constant, k_{cat}/K_m (6, 7). In studies on T7 DNA polymerase and HIV RT, it was shown that when the rate of chemistry is reduced by mutation or when incorporating a mismatch or a nucleoside analog, the binding steps come to equilibrium (6, 7). Accordingly, the slow rate of incorporation suggests that binding comes to equilibrium with the Y955C mutation, implying a significant affect of the Y955C mutation on nucleotide binding (Fig. 2 and Table 2).

The Y955C mutation resulted in reduced rate of polymerization and a decrease in the k_{cat}/K_m for correct incorporation. The effect of the mutation on the maximum rates of polymerization varied from 1.5- to 20-fold for correct incorporation (Table 2). However, the catalytic efficiencies (k_{cat}/K_m) were reduced 30 to 1300-fold. Thus, the effect of the Y955C mutation on the chemistry step was less significant and not correlated with the largest changes in k_{cat}/K_m. In particular, the specificity constant for incorporation of dATP:T was

reduced 1300-fold with only an eightfold reduction in k_{cat}. Thus, unlike wild-type enzyme, the specificity constant varied considerably for different base pairs. Perhaps the hydrogen bond network involving this tyrosine in the wild-type enzyme compensates for fewer hydrogen bonds in forming an A:T base pair compared to a G:C base pair, as suggested in early work on T7 DNA polymerase (14). Perhaps the stacking interaction between the tyrosine and the incoming base acts as an equalizer, allowing the rates of binding and polymerization to be less dependent on the type and size of the base. Cysteine is unable to compensate. Because of the positioning of Y955 (on the O-helix in T7 DNA polymerase), the interaction with the E895 residue may be critical in the ground state binding of the incoming nucleotide. The hydroxyl group of the tyrosine may stabilize the carboxyl group of the glutamate in the active site. In the T7 DNA polymerase, this glutamate selectively stabilizes the incoming TTP of a T:A base pair (14). This interaction may be reflected in Y955C pol γ as an increased K_m for TTP or dATP and reduced rates of catalysis.

Another significant detrimental effect of the Y955C mutation is reduced fidelity. The biggest drop in fidelity occurred between a T:T mismatch from one error in 260,000 for wild-type compared to one in 2,200 for the Y955C mutant. This 120-fold decrease in fidelity may contribute to the physiological consequences of this mutation. While replicating DNA, the Y955C mutant slows when reaching a T in the template and one time in 2,200 it will incorporate a T:T mismatch. Perhaps equally important, we show that the Y955C mutant catalyzes multiple misincorporation events, unlike the wild-type enzyme (27).

We have also studied the kinetics of incorporating 8-oxo-dGTP opposite dC and dA in the template. Our single-turnover experiments suggest not only a low discrimination against 8-oxo-deoxygyanosine, but that the level of discrimination is greater against a 8-oxo-dGTP:dA misincorporation (Table 4) for Y955C compared to wild-type enzyme. The wild-type enzyme has an unusual mechanism to minimize incorporation of 8-oxo-dGTP opposite a dCMP base, creating an equilibrium by slowing the release of pyrophosphate and allowing time for the reverse reaction to compete with product release (21). This resulted in a nucleotide dependence of amplitude and ultimately slowing the k_{cat} (Fig. 5C.). However, with the Y955C mutation, there was no evidence for the slow pyrophosphate release, but discrimination is lowered due to weaker nucleotide binding.

Physiological effects

The Y955C mutation leads to an autosomal dominant phenotype, but the effects are delayed in onset. Although referred to as “early onset PEO”, symptoms do not appear until the patients are in their thirties. Thus mtDNA replication is sufficient for individuals to live normally but then develop symptoms later in life. It is perhaps surprising that such drastic effects on the kinetics of incorporation are not lethal. Here we can only speculate about the relationship between the enzymology of pol γ and the physiological consequences of mutations. We presume that both mutant polymerase and a wild-type polymerase are present in the same mitochondrion, and perhaps mechanisms that regulate mtDNA copy number somehow compensate for the defective polymerase by allowing the wild-type enzyme to do most of the replication. Nonetheless, the drastic effects on catalytic efficiency and fidelity could ultimately cause the large deletions that are present in mtDNA in PEO patients by slowing the rate of replication such that replication stalls at long T tracks (16, 17, 39). More importantly perhaps, mutations introduced by the defective enzyme would be passed on to subsequent generations of mtDNA replication. Accordingly, it is possible that defects leading to reduced fidelity are more important than defects leading to slower rates of polymerization. While feedback mechanisms could compensate for reduced rates, mutations introduced during each round of replication accumulate over time and could explain the delayed onset of the disease. Increased mutation frequency can lead to defects in mtDNA that lead to increased oxidative stress, which in turn could lead to increased accumulation of

defects in the mtDNA. The accumulation of mutations may result in more severe symptoms such as Parkinson's and premature ovarian failure (17, 29). The dual expression of both the Y955C and wild-type polymerase allow for some level of faithful replication and likely prevents all out failure of mtDNA replication.

A recent report noted phenomena suggesting that the replication complex stalls at A:T tracks (40). Our results provide quantitative data to support the proposed slower rate of replication at dATP:T base pairs. However, simple stalling of the replication complex may not produce the observed physiological effects if other regulatory mechanisms compensate for the reduced number of active replisomes. Alternatively, stalled intermediates could lead to the accumulation of deletions in the mtDNA. Further studies of the polymerase need to be done in the presence of the complete replisome to fully understand these dynamics.

Acknowledgments

This work was supported by a grant from the National Institutes of Health (GM044613) and by the Welch Foundation (F-1604).

KinTek Corporation provided the RQF-3 rapid quench-flow instrument and the KinTek Explorer software.

ABBREVIATIONS

PEO	progressive external opthalmoplegia
pol γ	mitochondrial DNA polymerase
mtDNA	mitochondrial DNA

References

1. Taylor RW, Turnbull D. Mitochondrial DNA Mutations in Human Disease. Nature Reviews. 2005; 6:14.
2. Wong LJ, Naviaux RK, Brunetti-Pierri N, Zhang Q, Schmitt ES, Truong C, Milone M, Cohen BH, Wical B, Ganesh J, Basinger AA, Burton BK, Swoboda K, Gilbert DL, Vanderver A, Saneto RP, Maranda B, Arnold G, Abdenur JE, Waters PJ, Copeland WC. Molecular and clinical genetics of mitochondrial diseases due to POLG mutations. Hum Mutat. 2008; 29:E150–172. [PubMed: 18546365]
3. Lewis W, Day BJ, Kohler JJ, Hosseini SH, Chan SS, Green EC, Haase CP, Keebaugh ES, Long R, Ludaway T, Russ R, Steltzer J, Tioleco N, Santoianni R, Copeland WC. Decreased mtDNA, oxidative stress, cardiomyopathy, and death from transgenic cardiac targeted human mutant polymerase. Laboratory Investigation. 2007; 87:9.
4. Kaguni LS. DNA polymerase gamma, the mitochondrial replicase. Annu Rev Biochem. 2004; 73:293–320. [PubMed: 15189144]
5. Lee YS, Kennedy WD, Yin YW. Structural insight into processive human mitochondrial DNA synthesis and disease-related polymerase mutations. Cell. 2009; 139:312–324. [PubMed: 19837034]
6. Tsai YC, Johnson KA. A new paradigm for DNA polymerase specificity. Biochemistry. 2006; 45:9675–9687. [PubMed: 16893169]
7. Kellinger MW, Johnson KA. Nucleotide-dependent conformational change governs specificity and analog discrimination by HIV reverse transcriptase. Proc Natl Acad Sci U S A. 2010; 107:7734–7739. [PubMed: 20385846]
8. Johnson KA. Conformational coupling in DNA polymerase fidelity. Annu Rev Biochem. 1993; 62:685–713. [PubMed: 7688945]
9. Kati WM, Johnson KA, Jerva LF, Anderson KS. Mechanism and fidelity of HIV reverse transcriptase. J Biol Chem. 1992; 267:25988–25997. [PubMed: 1281479]

10. Johnson KA. The kinetic and chemical mechanism of high-fidelity DNA polymearases. Biochemica et Biophysica Acta. 2010; 1804:1041–1048.
11. Doublie S, Tabor S, Long AM, Richardson CC, Ellenberger T. Crystal structure of a bacteriophage T7 DNA replication complex at 2.2 A resolution. Nature. 1998; 391:251–258. [PubMed: 9440688]
12. Graziewicz MA, Longley MJ, Bienstock RJ, Zeviani M, Copeland WC. Structure-function defects of human mitochondrial DNA polymerase in autosomal dominant progressive external ophthalmoplegia. Nature Structural & Molecular Biology. 2004; 11:770–776.
13. Batabyal D, McKenzie JL, Johnson KA. Role of histidine 932 of the human mitochondrial DNA polymerase in nucleotide discrimination and inherited disease. J Biol Chem. 2010; 285:34191–34201. [PubMed: 20685647]
14. Donlin MJ, Johnson KA. Mutants Affecting Nucleotide Recognition by T7 DNA Polymerase. Biochemistry. 1994; 33:9.
15. Van Goethem G, Martin JJ, Van Broeckhoven C. Progressive external ophthalmoplegia and multiple mitochondrial DNA deletions. Acta Neurol Belg. 2002; 102:39–42. [PubMed: 12094562]
16. Luoma PT, Luo N, Loscher WN, Farr CL, Horvath R, Wanschitz J, Kiechl S, Kaguni LS, Suomalainen A. Functional defects due to spacer-region mutations of human mitochondrial DNA polymerase in a family with an ataxia-myopathy syndrome. Hum Mol Genet. 2005; 14:1907–1920. [PubMed: 15917273]
17. Pagnamenta AT, Taanman JW, Wilson CJ, Anderson NE, Marotta R, Duncan AJ, Bitner-Glindizicz M, Taylor RW, Laskowski A, Thorburn DR, Rahman S. Dominant inheritance of premature ovarian failure associated with mutant mitochondrial DNA polymerase gamma. Human Reproduction. 2006; 21:6.
18. Baruffini ELT, Dallabona C, Puglisi A, Zeviani M, Ferrero I. Genetic and chemical rescue of the Saccharomyces cerevisiae phenotype induced by mitochondrial DNA polymerase mutations associated with progressive external ophthalmoplegia in humans. Human Molecular Genetics. 2006; 15:9.
19. Ponamerev MV, Longley MJ, Nguyen D, Kunkel TA, Copeland WC. Active Site Mutation in DNA Polymerase Gamma Associated with Progressive External Opthalmoplegia Causes Error-prone DNA synthesis. Journal of Biological Chemistry. 2002; 277:3.
20. Pursell ZF, McDonald JT, Mathews CK, Kunkel TA. Trace amounts of 8-oxo-dGTP in mitochondrial dNTP pools reduce DNA polymerase gamma replication fidelity. Nucleic Acids Research. 2008; 36:7.
21. Hanes JW, Thal DM, Johnson KA. Incorporation and replication of 8-oxo-deoxyguanosine by the human mitochondrial DNA polymerase. J Biol Chem. 2006; 281:36241–36248. [PubMed: 17005553]
22. Longley MJ, Graziewicz MA, Bienstock RJ, Copeland WC. Consequences of mutations in human DNA polymerase gamma. Gene. 2005; 354:125–131. [PubMed: 15913923]
23. Copeland WC. Consequences of mutations in DNA polymerase gamma. Environmental and Molecular Mutagenesis. 2004; 44:193–193.
24. Johnson KA, Simpson ZB, Blom T. Global Kinetic Explorer: A new computer program for dynamic simulation and fitting of kinetic data. Anal Biochem. 2009; 387:20–29. [PubMed: 19154726]
25. Johnson KA, Simpson ZB, Blom T. FitSpace Explorer: An algorithm to evaluate multidimensional parameter space in fitting kinetic data. Anal Biochem. 2009; 387:30–41. [PubMed: 19168024]
26. Johnson AA, Tsai YC, Graves SW, Johnson KA. Human mitochondrial DNA polymerase holoenzyme: Reconstitution and characterization. Biochemistry. 2000; 39:1702–1708. [PubMed: 10677218]
27. Johnson AA, Johnson KA. Fidelity of nucleotide incorporation by human mitochondrial DNA polymerase. J Biol Chem. 2001; 276:38090–38096. [PubMed: 11477093]
28. Lee HR, Johnson KA. Fidelity of the human mitochondrial DNA polymerase. J Biol Chem. 2006; 281:36236–36240. [PubMed: 17005554]
29. Graziewicz M, Bienstock RJ, Copeland WC. The DNA polymerase gamma Y955C disease variant associated with PEO and parkinsonism mediates the incorporation and translesion synthesis opposite 7, 8-dihydro-8-oxo-2′-deoxyguanosine. Human Molecular Genetics. 2007; 16:10.

30. Graziewicz MA, Bienstock RJ, Copeland WC. The DNA polymerase gamma Y955C disease variant associated with PEO and parkinsonism mediates the incorporation and translesion synthesis opposite 7,8-dihydro-8-oxo-2′-deoxyguanosine. Hum Mol Genet. 2007; 16:2729–2739. [PubMed: 17725985]

31. Johnson AA, Ray AS, Hanes J, Suo ZC, Colacino JM, Anderson KS, Johnson KA. Toxicity of antiviral nucleoside analogs and the human mitochondrial DNA polymerase. Journal of Biological Chemistry. 2001; 276:40847–40857. [PubMed: 11526116]

32. Lim SE, Copeland WC. Differential incorporation and removal of antiviral deoxynucleotides by human DNA polymerase gamma. J Biol Chem. 2001; 276:23616–23623. [PubMed: 11319228]

33. Boosalis MS, Petruska J, Goodman MF. DNA polymerase insertion fidelity. Gel assay for site-specific kinetics. J Biol Chem. 1987; 262:14689–14696. [PubMed: 3667598]

34. Bertram JG, Oertell K, Petruska J, Goodman MF. DNA polymerase fidelity: comparing direct competition of right and wrong dNTP substrates with steady state and pre-steady state kinetics. Biochemistry. 2010; 49:20–28. [PubMed: 20000359]

35. Patel SS, Wong I, Johnson KA. Pre-Steady-State Kinetic-Analysis of Processive Dna-Replication Including Complete Characterization of An Exonuclease-Deficient Mutant. Biochemistry. 1991; 30:511–525. [PubMed: 1846298]

36. Hanes JW, Johnson KA. Real-time measurement of pyrophosphate release kinetics. Anal Biochem. 2008; 372:125–127. [PubMed: 17905190]

37. Hanes JW, Johnson KA. A novel mechanism of selectivity against AZT by the human mitochondrial DNA polymerase. Nucleic Acids Res. 2007; 35:6973–6983. [PubMed: 17940100]

38. Johnson KA. Role of induced fit in enzyme specificity: a molecular forward/reverse switch. J Biol Chem. 2008; 283:26297–26301. [PubMed: 18544537]

39. Atanassova N, Fuste JM, Wanrooij S, Macao B, Goffart S, Backstrom S, Farge G, Khvorostov I, Larsson NG, Spelbrink JN, Falkenberg M. Sequence-specific stalling of DNA polymerase {gamma} and the effects of mutations causing progressive ophthalmoplegia. Hum Mol Genet. 2011

40. Atanassova N, Fuste JM, Wanrooij S, Macao B, Goffart S, Backstrom S, Farge G, Khvorostov I, Larsson NG, Spelbrink JN, Falkenberg M. Sequence-specific stalling of DNA polymerase gamma and the effects of mutations causing progressive ophthalmoplegia. Hum Mol Genet. 2011; 20:1212–1223. [PubMed: 21228000]

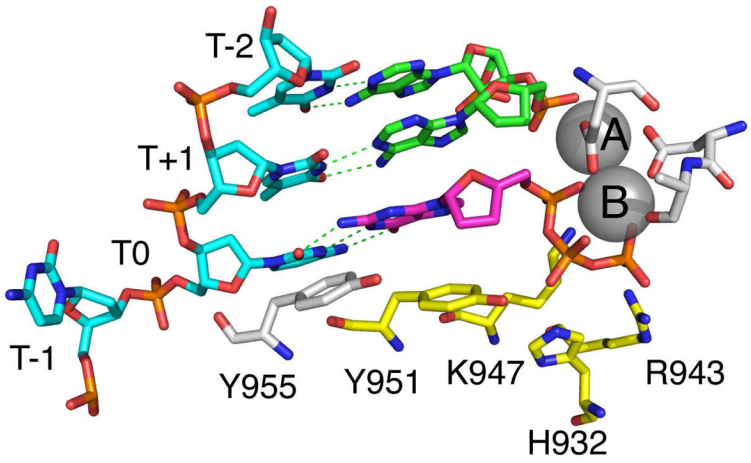

Fig. 1.

Position of Y955 at the Pol active site. Residue Y955 is shown in white CPK colors while the incoming nucleotide is magenta, the template strand is cyan and the primer is green. Active site residues with homology to residues in the T7 DNA polymerase structure are shown based upon the structure of T7DNA polymerase ternary complex ((11), PDB 1T7P) with residue numbers corresponding to the pol γ structure

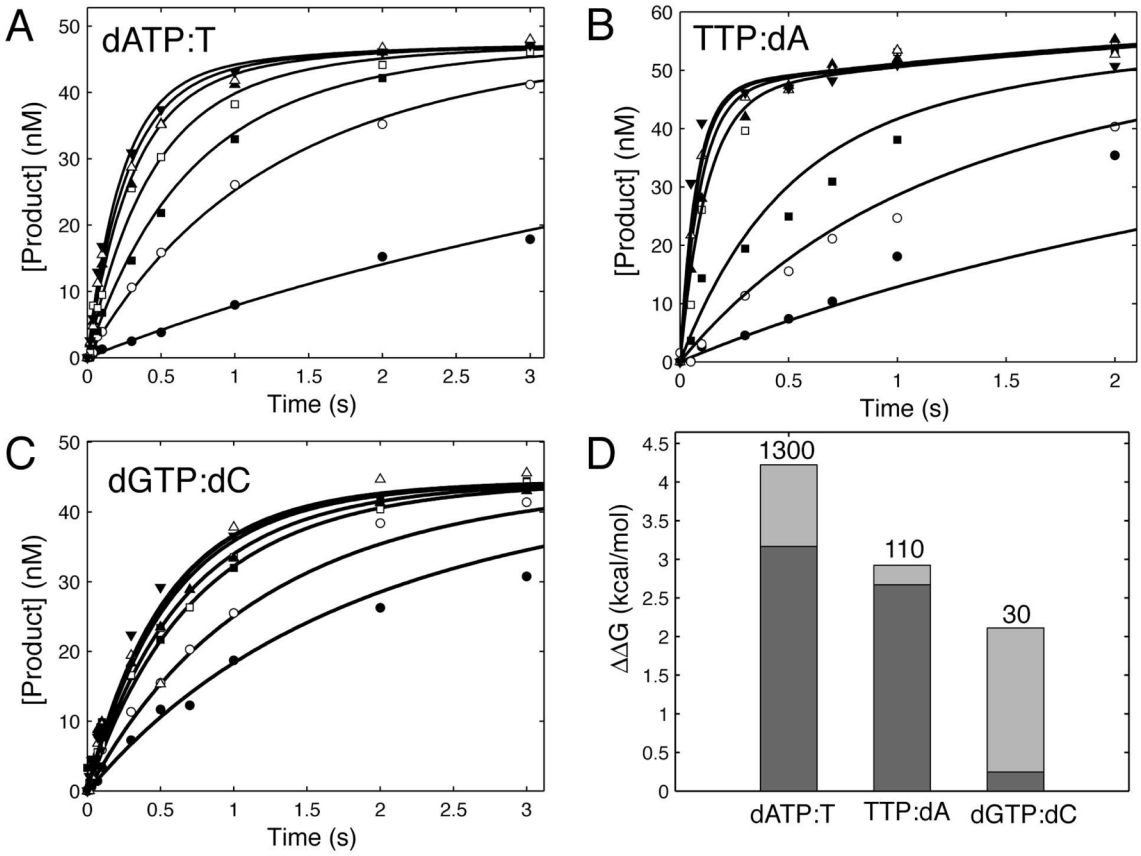

Fig. 2.

Kinetics of correct base-pair incorporation. For each experiment, a preformed enzyme-DNA complex was rapidly mixed with Mg^{2+} and various concentrations of dATP, dCTP, dGTP or TTP. In each experiment, the final concentrations of the enzyme and DNA after mixing were 100–150 nM and 70 nM, respectively. In globally fitting each data set, the concentration of active enzyme was adjusted slightly to fit the amplitude. (A) Incorporation of dATP:T for Y955C exo- pol γ at 5 (●), 25 (○), 50 (■), 100 (□), 200 (▲), 300 (△), 500 (▼) μM was globally fit to yield a k_{cat} of 5.4 ± 0.45 s^{-1} and a K_m of 120 ±15 μM. (B) Formation of a TTP:dA base pair with the Y955C exo- pol γ at various concentrations of TTP (1 (●), 3 (○), 7 (■), 50 (□), 100 (▲), 200 (△), 300 (▼) μM) was globally fit to Scheme 1 to yield a k_{cat} of 16.6 ± 3.1 s^{-1} and a K_m of 46 ± 11 μM. (C) Formation of a dGTP:dC base pair with the Y955C exo- pol γ at various concentrations of dGTP (0.5 (●), 1 (○), 3 (■), 5 (□), 15 (▲), 50 (△), 150 (▼) μM) was globally fit to yield a k_{cat} of 1.8 ± 0.18 s^{-1} and a K_m of 1.2± 0.32 μM. (D) The change in the specificity constant for each correct base pair incorporation relative to wild type is shown on a free energy scale. The numbers above each bar give the fold change in k_{cat}/K_m in comparing wild-type with the Y955C mutant. Contributions arising from k_{cat} (light) and K_m (dark) were calculated as described in the methods.

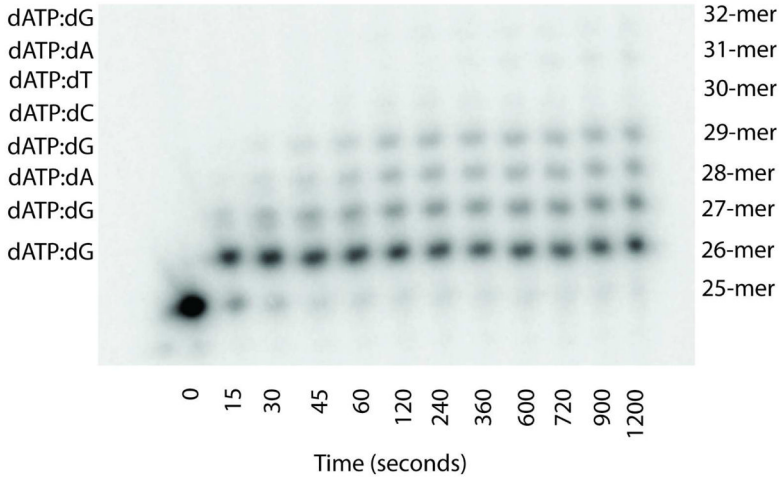

Fig. 3.

Multiple misincorporation events. Products from misincorporation of dGTP (at 1000 μM) onto a templating T catalyzed by Y955C exo- pol γ were separated on a 15% acrylamide/ 7M denaturing PAGE gel to visualize the formation of multiple misincorporation products product over time. The text on the left gives the identity of the dNTP and templating corresponding to each incorporation. For example, dATP:dG refers to misincorporation of dATP opposite dG in the template.

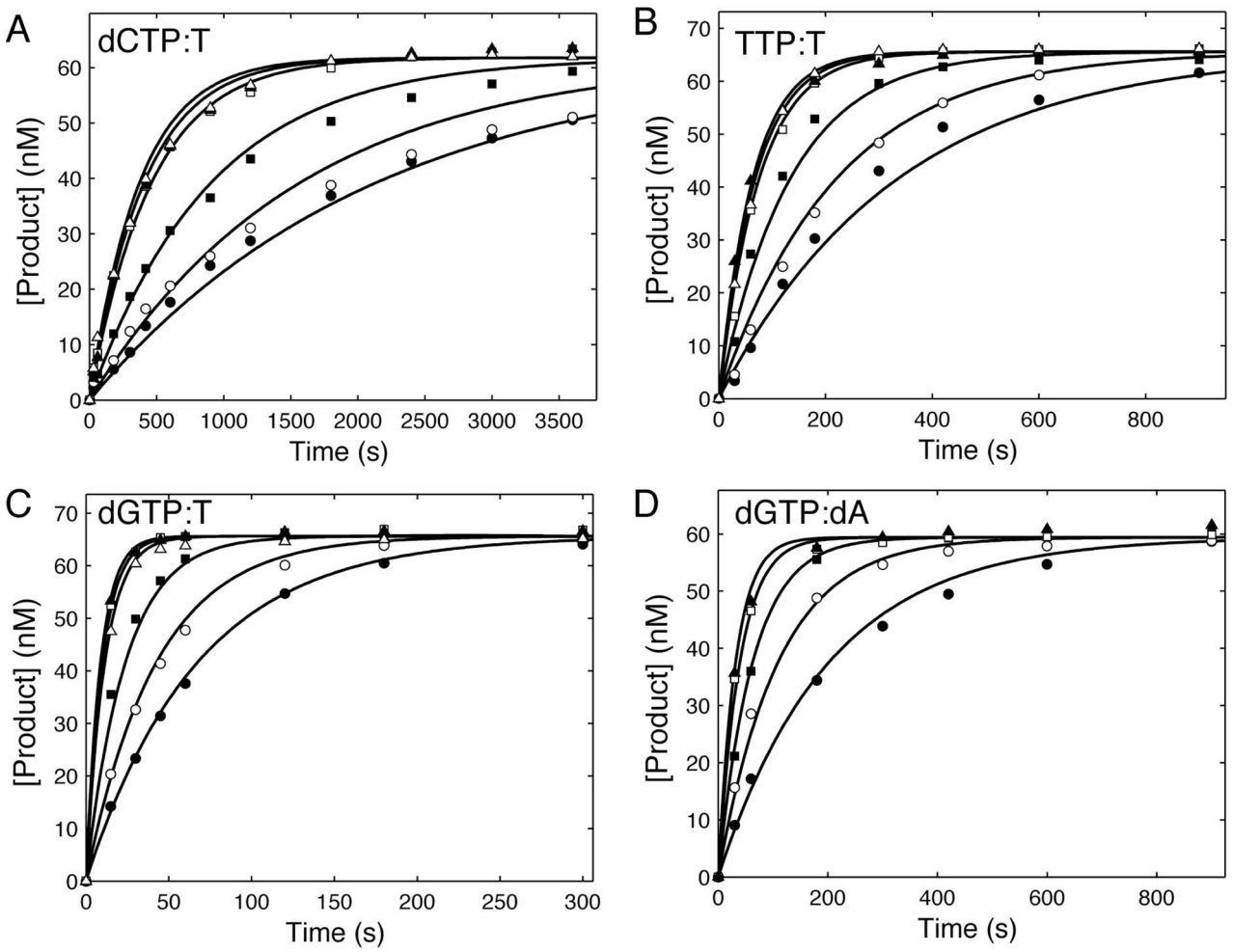

Fig. 4.

Kinetics of misincorporation. For each experiment, a preformed enzyme-DNA complex ([enzyme] > [DNA duplex]) was rapidly mixed with Mg^{2+} and various concentrations of nucleotide. In each experiment, the final concentrations of the enzyme and DNA after mixing were 100–150 nM and 70 nM, respectively. In globally fitting each data set, the concentration of active enzyme was adjusted slightly to fit the amplitude. (A) Formation of a dCTP:T mismatch by Y955C exo- pol γ at 300 (●), 500 (○), 1000 (■), 3000 (□), 4000 (▲), 5000 (△) μM was fit globally to yield a k_{cat} of 0.004 ± 0.002 s^{-1} and a K_m of 2020 ± 148 μM. (B) Formation of a TTP:T mismatch by Y955C exo- pol γ at each concentration of TTP (300 (●), 500 (○), 1000 (■), 3000 (□), 4000 (▲), 5000 (△) μM) was globally fit to yield k_{cat} of 0.022 ± 0.0050 s^{-1} and a K_m of 1360 ± 138 μM. (C) Formation of a dGTP:T mismatch by Y955C exo- pol γ at each concentration of dGTP (300 (●), 500 (○), 1000 (■), 3000 (□), 4000 (▲), 5000 (△) μM) was globally fit to yield a k_{cat} of 0.22 ± 0.024 s^{-1} and a K_m of 2950 ± 397 μM. (D) Formation of a dGTP:dA base pair with Y955C exo- pol γ (25 (●), 50 (○), 100 (■), 200 (□), 300 (▲)) was globally fit to Scheme 1 to yield a k_{cat} of 0.064±.014 s^{-1} and a K_m of 217.1±31.18 μM. In each figure, the smooth lines show the fitted curves derived by global fitting using KinTek Explorer software (24, 25).

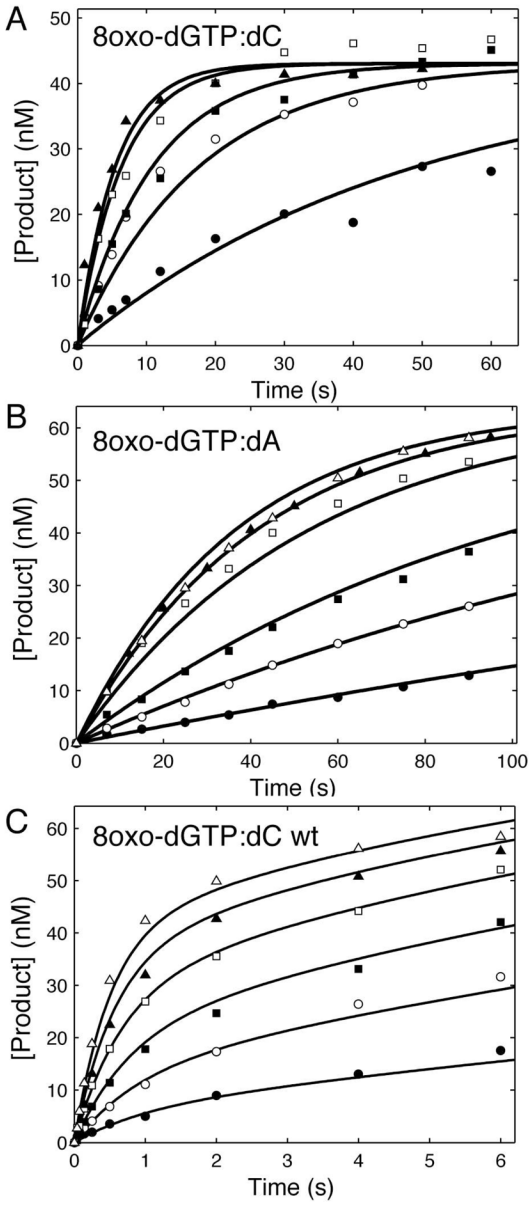

Fig. 5.

Kinetics of incorporation of 8-oxo-dGTP. For each experiment, a preformed enzyme-DNA complex ([enzyme] > [DNA duplex]) was rapidly mixed with Mg^{2+} and various concentrations of TTP, dGTP, or 8-oxo-dGTP. In each experiment, the final concentrations of the enzyme and DNA after mixing were 100–150 nM and 70 nM, respectively. In globally fitting each data set, the concentration of active enzyme was adjusted slightly to fit the amplitude. (A) Formation of 8-oxo-dG:dC base pair with the Y955C exo- pol γ at various concentrations of 8-oxo-dGTP (5 (●), 15 (○), 50 (■), 100 (□), 300 (▲), 500 (△) μM) was globally fit to Scheme 1 to yield a k_{cat} of 0.28 ± 0.049 s^{-1} and a K_m of 163± 42.1 μM. (B) Formation of 8-oxo-dG:dA base pair with the Y955C exo- pol γ at various concentrations of 8-oxo-dGTP (10 (●), 25 (○), 50 (■), 150 (□), 300 (▲), 500 (△) μM) was globally fit to Scheme 1 to yield a k_{cat} of 0.035± 0.005 s^{-1} and a K_m of 95 ± 11 μM. (C) Formation of a 8-oxo-dG:dC base pair (10 (●), 25 (○), 50 (■), 100 (□), 200 (▲), 400 (△) μM 8-oxo-dGTP) with wild-type exo- pol γ fit globally to Scheme 2 to derive the

following: $K_{d,1}$ = 135 ± 15 μM, k_2 = 1.6 ± 0.14 s^{-1}, k_{-2} = 0.7 ± 0.15 s^{-1} and k_3 = 0.23 ± 0.06 s^{-1}. Data are from (21). In each figure, the smooth lines show the fitted curves derived by global fitting using KinTek Explorer software (24, 25). Data fitting by conventional means provided estimates of $K_{d,1}$ = 135 μM, k_2 = 2 s^{-1}, k_{-2} = 0.7 and k_3 = 0.4 s^{-1}(21). Thus, the rate constants derived by both methods are comparable, but the confidence in the fitting derived by simulation is greater because it includes both rate and amplitude data in a single fitting step rather than by a complex combination of plots of rate and amplitudes as a function of concentration.

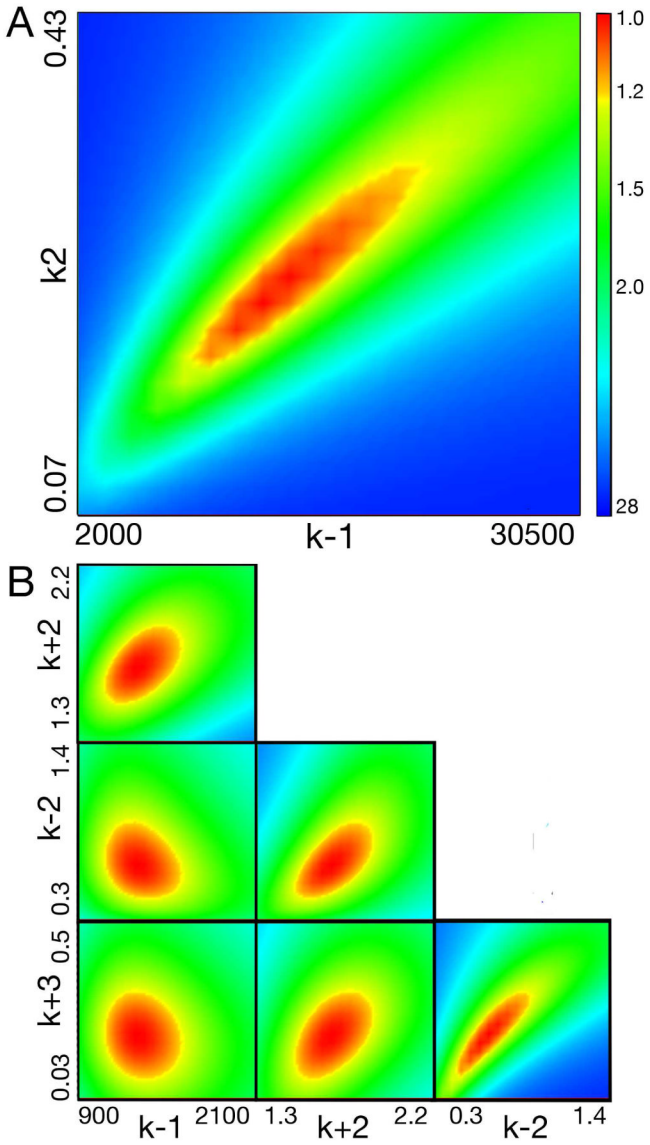

Fig. 6.

Confidence contours. A. The relationship between the total chi^2 and the two kinetic parameters k_2 (k_{cat}) and k_{-1} ($K_m = k_{-1}/k_1$) is shown with the color scale ranging from red (best fit) to blue. The scale is based upon the ratio of chi^2 divided by the minimum chi^2. A threshold at 1.2 provides upper and lower limits for each parameter (25) defined by the yellow band. Note that the ratio of the two parameters (defining k_{cat}/K_m) is known with greater certainty than either parameter individually. B. Confidence contours for fitting data in Fig. 5C from (21). The color scale is identical to that in A. The contours demonstrate that all four parameters are well constrained.

$$ED_n + N \underset{}{\overset{K_d}{\rightleftarrows}} ED_nN \overset{k_{pol}}{\rightleftarrows} ED_{n+1} + PP_i$$

Scheme 1.

$$ED_n + N \underset{}{\overset{K_d}{\rightleftharpoons}} ED_nN \underset{k_{-2}}{\overset{k_2}{\rightleftharpoons}} ED_{n+1}PP_i$$

$$ED_{n+1}PP_i \overset{k_3}{\rightleftharpoons} ED_{n+1} + PP_i$$

Scheme 2.

Table 1

Primer and Template sequences used for single turnover experiments[a]

Oligo	nt	Sequence
Primer	25	5′GCCTCGCAGCCGTCCAACCAACTCA 3′
Template 1	45	5′GGACGGCATTGGATCGAGGTTGAGTTGGTTGGACGGCTGCGAGGC 3′
Template 2	45	5′GGACGGCATTGGATCGAGTCTGAGTTGGTTGGACGGCTG CGAGGC 3′
Template 3	45	5′GGACGGCATTGGATCGAGTATGAGTTGGTTGGACGGCTGCGAGGC 3′

[a]Primer and template sequences of oligonucleotide (Oligo) used in single-turnover experiments. The length is given in nucleotides (nt). The underlined base is the templating base for the incoming nucleotide.

Table 2

Effect of pol γ Y955C on correct base pair incorporation kinetics

		k_{cat}	K_m	k_{cat}/K_m	Fold effect
	base pair	**s^{-1}**	**μM**	**$\mu M^{-1}s^{-1}$**	
Y955C	dATP:T	5.4 ± 0.45	120 ± 15	0.044 ± 0.006	1300
	dGTP:dC	1.8 ± 0.18	1.2 ± 0.3	1.5 ± 0.4	30
	TTP:dA	17 ± 3	46 ± 11	0.35 ± 0.1	110
WT[b]	dATP:T	45 ± 1	0.8 ± 0.06	57 ± 5	
	dGTP:dC	37 ± 2	0.8 ± 0.12	46 ± 7	
	TTP:dA	25 ± 2	0.6 ± 0.16	40 ± 10	

[a]Kinetic parameters were derived in fitting the data in Fig. 2. The fold effect on k_{cat}/K_m was calculated from values for the wild-type divided by k_{cat}/K_m from the mutant.

[b]Values for the wild-type were previously determined (28).

Biochemistry. Author manuscript; available in PMC 2012 July 26.

Table 3

Effect of the Y955C mutation of kinetic parameters governing fidelity[a]

		k_{cat}	K_m	k_{cat}/K_m	D
	base pair	**s^{-1}**	**μM**	**$\mu M^{-1}s^{-1}$**	
Y955C	dATP:T	5.4 ± 0.45	120 ± 15	0.044 ± 0.0064	--
	dGTP:T	0.22 ± 0.02	3000 ± 400	0.00008 ± 0.00001	550
	dCTP:T	0.004 ± 0.002	2020 ± 150	0.000002 ± 0.000001	22,000
	TTP:T	0.022 ± 0.0050	1360 ± 140	0.00002 ± 0.000004	2,200
	dGTP:dA	0.06 ± 0.01	220 ± 30	0.0003 ± 0.00006	7,500
WT[b]	dATP:T	45 ± 1	0.8 ± 0.06	56 ± 4	--
	dGTP:T	1.16 ± 0.06	70 ± 10	0.16 ± 0.003	3,500
	dCTP:T	0.038 ± 0.003	360 ± 80	0.001 ± 0.00002	570,000
	TTP:T	0.013 ± 0.0003	57 ± 5	0.0002 ± 0.00002	260,000
	dGTP:dA	<0.1	>1000	0.0001	390,000

[a]Kinetic parameters were derived in fitting the data in Fig. 4. Discrimination (D) was calculated as the ratio of k_{cat}/K_m values for correct versus mismatched base pairs.

[b,c]Values for the wild-type enzyme were determined previously (27, 28).

Table 4

Effect of the pol γ Y955C mutation on incorporation of 8-oxo-dGTP[a]

	base pair	k_{cat}	K_m	k_{cat}/K_m	Fold Effect
		s^{-1}	μM	$\mu M^{-1}s^{-1}$	
Y955C	8-oxo-dGTP:dC	0.28 ± 0.05	160 ± 40	0.002 ± 0.0005	1.5
	8-oxo-dGTP:dA	0.035 ± 0.005	95 ± 11	0.0004 ± 0.00007	500
WT	8-oxo-dGTP:dC	0.15 ± 0.02	48 ± 8	0.003 ± 0.001	
	8-oxo-dGTP:dA[b]	0.62 ± 0.05	3.3 ± 1.0	0.20 ± 0.1	

[a] Values for k_{cat} and K_m were calculated from the individual rate constants as described in the methods.

[b] Values taken from (21).